RSC Advances

PAPER

Cite this: *RSC Adv.*, 2021, **11**, 8674

Low-cost and scalable carbon bread used as an efficient solar steam generator with high performance for water desalination and purification†

Yang Yang, *[a] Man Zhao,[a] Zhen Cao,[a] Zhen Ge,[b] Yanfeng Ma*[b] and Yongsheng Chen[b]

Solar steam generation has been considered as a promising method for water desalination and purification. Achieving a simple, scalable and cost-effective method to fabricate solar-thermal materials with high performance is the key for its widespread application. Herein, we demonstrate high performance "carbon bread" as a solar steam generator *via* a facile one-pot baking process, which can be carried out in most household kitchens in our daily life without high-temperature carbonization. The carbon bread could achieve ~85.9% conversion efficiency under 1 sun illumination and ~81.7% efficiency even under 0.25 sun. The highly efficient solar steam generation performance benefits from the unique structure and properties of carbon bread: efficient and broadband light absorption, 3D interconnected hierarchical pores, excellent hydrophilicity and thermal insulation. This scalable material could generate fresh drinkable water from seawater and wastewater under ambient conditions. The successful demonstration of this simple and easily accessible carbon bread material could inspire the development of solar-driven water evaporators derived from low cost and commercially available raw chemicals through a simple manufacturing process for practical water desalination and purification on a large scale.

Received 22nd January 2021
Accepted 11th February 2021

DOI: 10.1039/d1ra00592h

rsc.li/rsc-advances

1. Introduction

Water scarcity has been a severe global problem owing to the pressure of the continuously contaminated drinkable water resources and growing population.[1–3] Solar steam generation for water desalination and purification is viewed as a potential and sustainable technology to alleviate freshwater scarcity due to the free-energy consumption, low-cost and negligible impacts on the environment.[2–5] Based on this technology, an interfacial evaporation approach has been developed recently, which selectively heats the evaporative portion of water near the surface of the evaporator instead of the entire bulk water.[6–10] Therefore, this approach could avoid volumetric heating, minimize the solar-thermal material used, and accelerate the evaporation process.[6]

In the solar interfacial evaporation system, solar-thermal materials play a crucial role and an ideal absorber should satisfy several characteristics: strong and broadband light absorption, porosity, wettability, low costs and mechanical strength.[11–14] To this end, immense efforts have been dedicated to developing an advanced absorber to achieve the above properties.[13–26] So far, multitudinous materials including plasmonic metals,[13,15–18] carbon-based nanostructures,[14,19–21,27–29] semiconductors[22,23] and bio-inspired materials[24–26,30–32] have been investigated by researchers to boost the efficiency of solar energy harvesting further. For instance, Zhu's group[18] demonstrated a gold based plasmonic absorber, which has over 90% efficiency under 4 sun (4 kW m^{-2}) illumination. Hu and coworkers[24] proposed a "tree-inspired design" using natural wood with an efficiency of 57.3% at 1 sun to 80.4% at 10 sun. Recently, Yu's group[33] reported a hydrogel consisting of polyvinyl alcohol and chitosan with a record efficiency of 92% under 1 sun. While much progress and many approaches have been made, most of them have limitations[18,19,34,35] such as high costs, the lack of scalable features or complicated fabrication, which have been considered as big obstacles hindering their practical applications. In this context, it is highly challenging but also extremely desirable to develop a cost-effective and scalable solution to fabricate high-performance solar-thermal materials with simultaneous optimal light absorption, water transport and thermal management.[36–38]

Bread, which is familiar in our daily life, seems to be a surprising candidate for efficient solar steam generation, benefiting from the rich porous structure, excellent

[a]*The Institute of Seawater Desalination and Multipurpose Utilization, Ministry of Natural Resources (Tianjin), Tianjin 300192, China. E-mail: yangyang1990@mail.nankai.edu.cn*

[b]*The Centre of Nanoscale Science and Technology, Key Laboratory of Functional Polymer Materials, College of Chemistry, Nankai University, Tianjin 300071, China. E-mail: yanfengma@nankai.edu.cn*

† Electronic supplementary information (ESI) available. See DOI: 10.1039/d1ra00592h

hydrophilicity, non-toxicity and high technical maturity for large-scale preparation. Here, for the first time, we report "carbon bread" as a solar steam generator fabricated *via* a facile method, the same as making bread in our daily life. In the carbon bread, bread was selected as a skeleton, and carbon black was introduced into the bread to enhance the absorbance due to its high absorption and low cost.[39,40] This low-cost ($0.85 per m^2) and scalable carbon bread sponge could be directly utilized as a high-performance evaporator for solar steam generation, with a high water production rate of 1.28 kg h^{-1} m^{-2} and 85.9% energy efficiency under 1 sun solar illumination. This high performance benefits from the 3D interconnected hierarchical pores, hydrophilicity and thermal insulation properties of the bread, as well as the high light absorption capability of the carbon black. More importantly, using this simple ready-to-use material, the solar energy conversion efficiency can reach 81.7% under ambient sunlight (0.25 sun). Considering the low cost, easy fabrication and high energy conversion efficiency, a scalable and efficient desalination/sewage treatment device was fabricated. From these results, this carbon bread device shows great potential to alleviate the water scarcity and could provide a new means for future design and the exploitation of high-performance and cost-efficient solar steam generators.

2. Materials and methods

2.1 Material preparation

As shown in Fig. 1 and S1,† a low-cost flour ($0.20 per lb) and carbon black particles ($0.45 per lb) were used as raw materials to prepare carbon bread without any special equipment through a classic and easy method,[41] involving simple kneading, foaming and baking processes. Finally, black carbon bread with a porous structure was obtained by the flour crosslinking and the uniform black color proved that the carbon black particles were well deposited on the carbon bread.

A series of carbon breads with different concentrations of carbon black were prepared (Table S1†). As a typical example, for the absorber CB-6, 30.0 g dry flour (all-purpose flour, Fulinmen COFCO) and 0.075 g carbon black (Tianjin Plannano Energy Technology Co. Ltd.) were well-mixed in a container firstly. 0.5 g yeast (Angel Yeast Co. Ltd.) was dissolved in 17 mL distilled water (30 °C) and then the flour, carbon black particles, yeast and water were stirred and kneaded together thoroughly until the dough was smooth and elastic. The mixture was sealed and put into an oven at 30 °C. After 2 hours of foaming, the dough inflated and was exhausted by kneading. Subsequently, the dough was transferred into a mold and re-foamed at 30 °C for 1 hour. Finally, the dough was baked in an oven at a temperature of 150 °C for 30 minutes. The as-prepared carbon bread was cut into a cuboid of 10 mm square and 20 mm thickness for use as the evaporator for solar steam generation.

This method is very convenient and highly technically mature and can be carried out in most household kitchens and even has realized fully automatic production using household automatic bread machines. Fig. 1 also shows a piece of carbon bread with a large size of 400 × 300 × 50 mm^3 to meet the practical requirement.

2.2 Evaporation experiment

The solar steam generation test was performed using a home-made testing system. The as-prepared carbon bread was integrated on polystyrene (PS) foam, and then put in the center of the chamber with the carbon bread immersed in bulk water. The testing system contains a solar simulator (SOFN, 7ILX500P), an IR camera (FLIR T630sc), an electronic balance (OHAUS, AX224ZH) and a temperature probe.

2.3 Material characterization

The morphology was characterized using a scanning electron microscope (Hitachi SU3500). The absorption of the materials was measured *via* the UV-Vis-NIR spectra (PE Lambda 750). The contact angles were measured *via* a contact angle meter (Biolin, Theta Lite). The surface composition was analyzed by Fourier transform infrared spectroscopy (FTIR, Thermo Instrument) and X-ray photoelectron spectroscopy (XPS, ESCALAB 250XI). X-ray diffraction (XRD) was performed on a Rigaku MiniFlex 600 diffractometer to analyze the structure. The content of ion was measured by inductively coupled plasma mass spectroscopy (ICP-MS, Agilent 7800). Specific surface area and pore size distribution of the material were measured on a Micromeritics AutoPore IV 9510 apparatus, using mercury intrusion porosimetry (MIP) and the results showed that the material has a BET surface area of ~70 m^2 g^{-1}.

3. Results and discussion

3.1 Material structure and properties

The as-prepared black carbon bread (CB, Fig. 2a) was elastic and robust (Fig. S2 and S3†) with a porous network, which is mainly

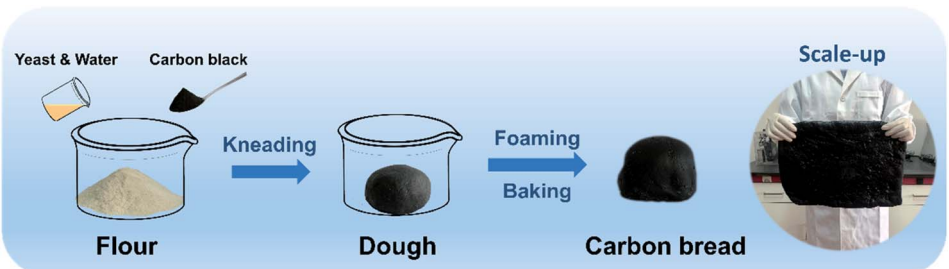

Fig. 1 Schematic illustration of the preparation of carbon bread.

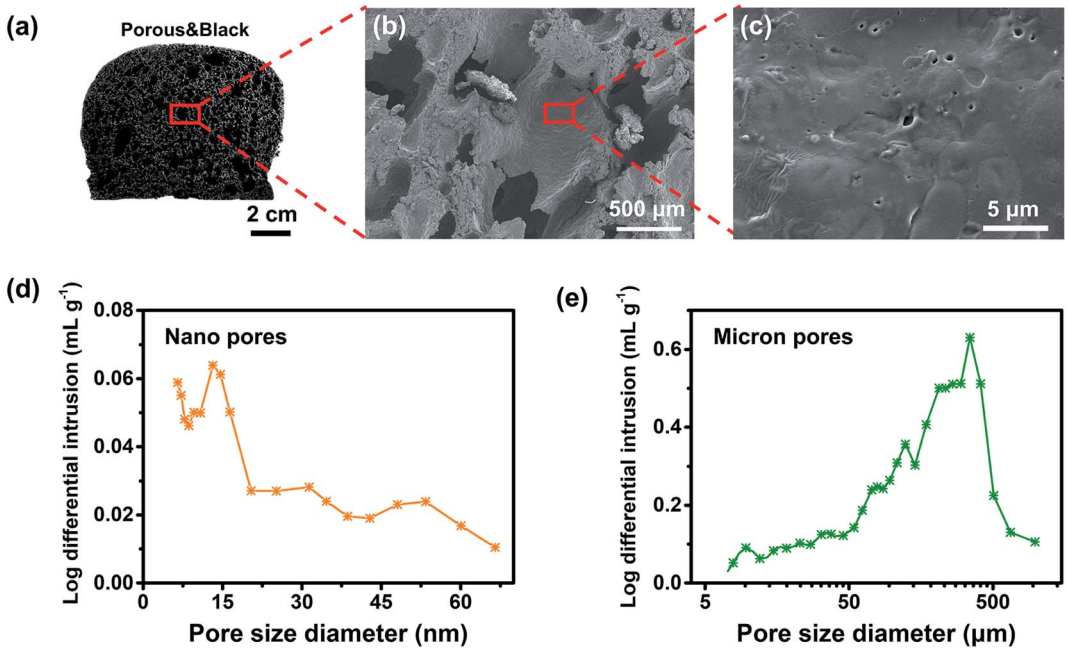

Fig. 2 (a) Optical image of CB (b and c) SEM images of the CB. Pore size distribution of the CB across (d) nanometer pores and (e) micron pores. The abundant nanometer pores and micron pores could provide channels for water transfer and increase the evaporation surface.

formed by the disulfide crosslinking of gliadin and glutenin proteins as well as the crosslinking of the starch and proteins in flour.[42] As can be seen from the XRD data (Fig. S4†), CB displayed the diffraction peaks of pure flour but the peaks were broader than those of flour, suggesting the crosslinking of flour.[43]

The morphology and microstructure of CB examined by SEM (Fig. 2b, c and S5†) showed a 3D crosslinking network structure with hierarchical pores (nanometer and micron pores) and interconnected channels formed by the cross-linked flour. This morphology makes CB exhibit low density (~0.2 g cm^{-3}) with a porosity of ~60%. Mercury intrusion porosimetry analysis (Fig. 2d and e) also demonstrated that the pores distributed in two ranges, nanometer pores of ~7–20 nm and micron pores of ~10–500 μm. The micron pores of carbon bread mainly provide convenient channels for water transfer and the nanometer pores may increase the evaporation surface, synergistically promoting the water evaporation.[44]

The surface contact angle measurement of CB is shown in Fig. 3a. As can be seen from the high-speed camera images, the water droplet rapidly immersed into the CB within 90 ms through capillary interaction, showing excellent hydrophilicity. Based on the FTIR (Fig. S6†) and XPS (Fig. S7†) results, the excellent wettability benefits from the abundant hydrophilic functional groups (–OH and –COOH), and is beneficial to the transport of water from the bottom to the evaporation surface.

Moreover, low thermal conductivity is important to the solar-thermal material for heat localization. The thermal conductivities of CB in air (dry state, Fig. 3b) and filled with water (wet state, Fig. 3c) were measured with an infrared (IR) microscope (see details in the ESI†).[14] The inset is a representative picture taken using an IR microscope indicating the temperature gradient. CB showed low thermal conductivity both in dry and wet states, indicating that it is favorable for localizing heat and showing great promise as a thermal insulating material in solar evaporation systems.

Above all, this porous structure formed by the crosslinking of flour could serve as a support, water transporter and thermal insulator simultaneously in a solar-driven evaporation device.

3.2 Evaporation enhanced by carbon bread

Efficient and broadband absorption of the absorber plays a critical role in the solar-thermal conversion performance.[19] Carbon black has a strong ability to absorb sunlight and affects the absorption of carbon bread. Here, a series of CBs with different concentrations of carbon black were prepared (Table S1†). As can be seen from Fig. 4a, the pristine bread without carbon black (CB-0) maintained the original yellow-white color of the flour, and the carbon bread gradually darkened with the addition of carbon black. The absorption characterization was carried out and showed that the absorption first increased gradually with the increase of carbon black addition and then remained unchanged when the carbon black/flour ratio was 1 : 400 (CB-6) with the highest optical absorption of 98% in almost all light wavelengths (200–2500 nm). It should also be noted that even without carbon black, CB-0 still has a higher absorption than the flour, over 52% in 500–1200 nm and over 80% in 1300–2500 nm (Fig. S8†), indicating that the porous structure could promote the absorption by multiple reflections.[45] Based on the above results, the high absorption comes from both the high intrinsic absorption of carbon black and the porous and rough structure of bread that restricts the scattering of light.

The carbon bread on the bulk water was exposed to solar illumination (1 sun) to examine the steam generation performance

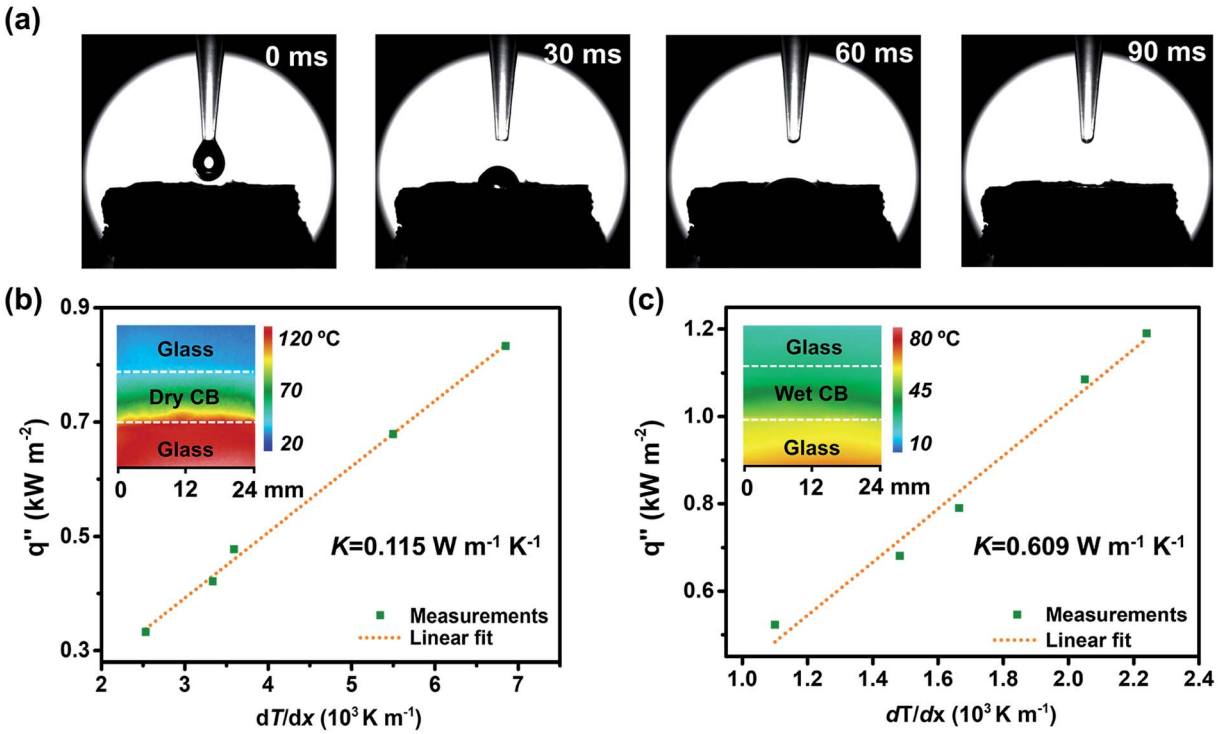

Fig. 3 (a) Contact angle images of the CB at different times. Thermal conductivities of the CB (b) in air (dry state) and (c) filled with water (wet state).

(Fig. S9†). The water evaporation over time with CBs was measured using a real-time balance. As can be seen from Fig. 4b, the water evaporation of different CBs under 1 sun illumination in an hour increased with the increase of the concentration of carbon black, showing the same trend of absorption. The result reveals that the absorption is directly proportional to the efficiency and is a prerequisite for efficient solar steam generation.

The typical curves of time-dependent water evaporation for pristine bread without carbon black (CB-0) and the optimal carbon bread (CB-6) under 1 sun are provided in Fig. 5a. The evaporation rates were calculated from the slope of the curves and the rate of water evaporation under a dark environment was subtracted. With CB-6, the water evaporation rate reached 1.28 kg m^{-2} h^{-1}, more than double that (0.62 kg m^{-2} h^{-1}) with CB-0 on water and five times that (0.25 kg m^{-2} h^{-1}) without materials on water. As shown in the right part of Fig. 5a, the surface temperature of water without the material was only 28.5 °C after illumination. While the surface temperature of CB-6 was up to above 34.0 °C, the water temperature underlying CB-6 still remained at around 26.4 °C. These results indicate the excellent solar-thermal conversion performance and little heat loss due to the low thermal conductivity of CBs.

The solar steam conversion efficiency (η) is defined as $\eta = \dot{m}h_{LV}/Aq_{solar}$, where $\dot{m}$ is the stable water evaporation rate, h_{LV} denotes the total enthalpy of the liquid–vapour phase change and sensible heat, A is the surface area of the material, and q_{solar} is the solar intensity.[20] The efficiency of CB-6 reached 85.9 ± 3.5% under 1 sun illumination, indicating its potential as an efficient solar steam generator.

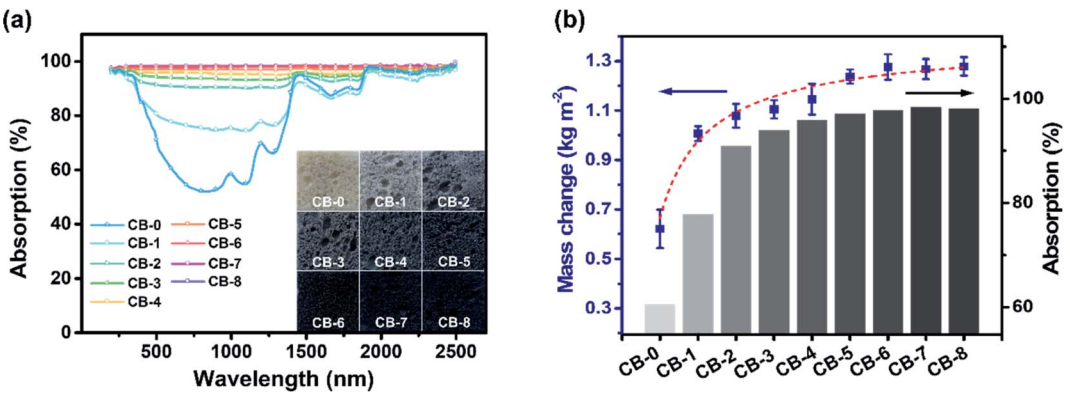

Fig. 4 (a) Optical image and absorption of carbon breads with different concentrations of carbon black. (b) Water mass change in an hour of CBs with different carbon black particle concentrations. Error bars: standard deviation (s.d.).

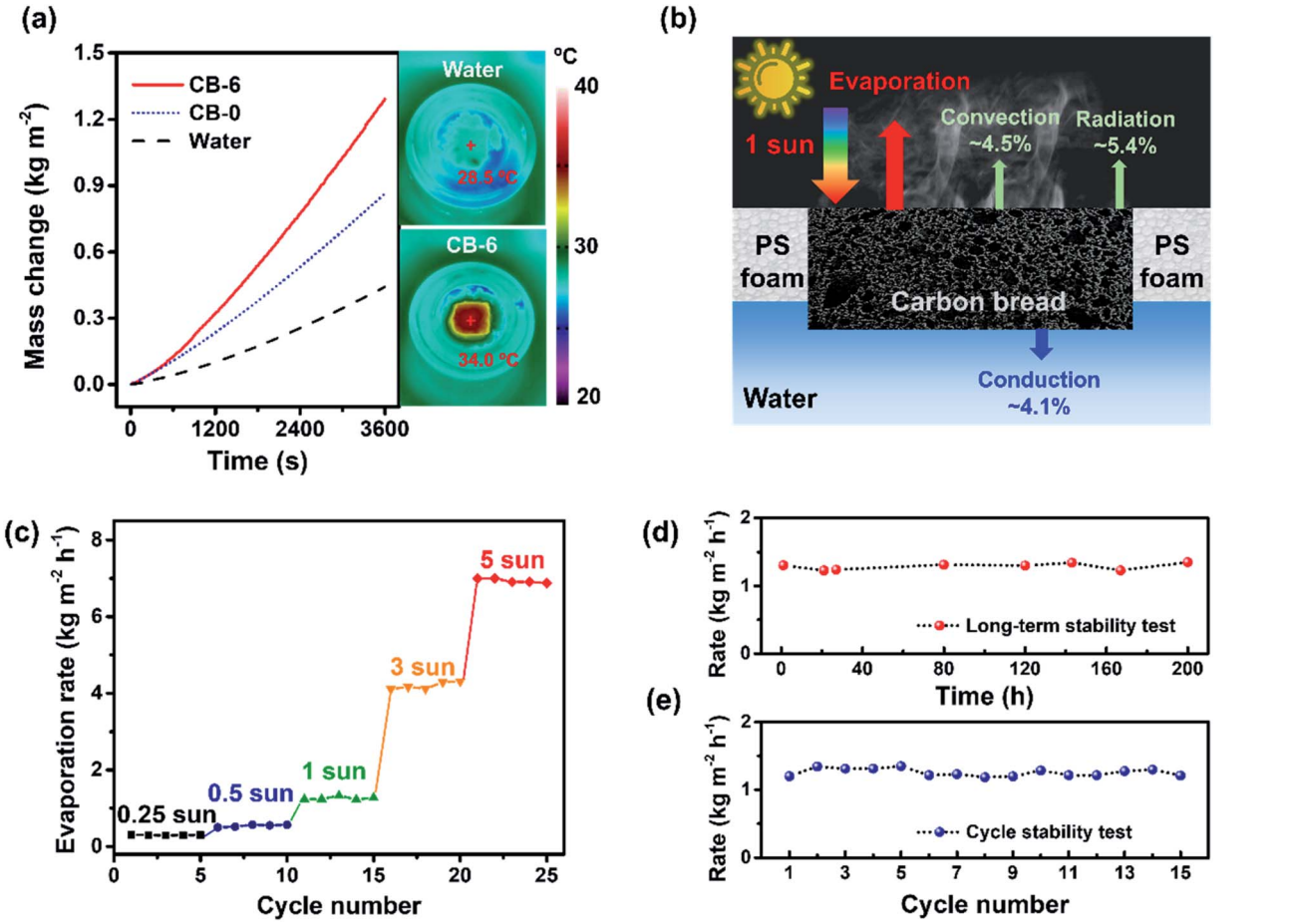

Fig. 5 (a) The left part is the mass change of water with CB-0 and CB-6 under 1 sun solar illumination and the case without CB; the right part shows the IR images under 1 sun with/without CB-6. (b) Diagram of heat transfer in the CB architecture. (c) Water evaporation rate under a series of light intensities. (d) Evaporation rate of CB-6 under 1 sun over 200 hours. (e) Reusability of CB-6 under 1 sun solar illumination for 15 cycles with NaCl solution.

3.3 Heat loss

The analysis of the heat transfer mechanism under 1 sun is shown in Fig. 5b. It involves radiative (~5.4%) and convective (~4.5%) heat loss to the ambient, and conductive (~4.1%) heat loss to the underlying water (detailed calculations are given in the ESI†).[19,20,29] First, the combination of the intrinsic strong and broad absorption of carbon black with the porous and rough structure ensures an efficient and broadband absorption in the entire sunlight wavelength. Then, the carbon bread could exchange the absorbed solar energy with the water to generate the steam efficiently due to the hydrophilicity and hierarchical pores. Furthermore, the low thermal conductivity profited from the porous structure makes this material effectively minimize the heat conduction to the underlying and surrounding water. Benefiting from all the above properties, carbon bread shows excellent performance in solar steam generation.

3.4 Effect of illumination intensity

The solar steam generation performance of CB-6 under different light intensities was evaluated (Fig. 5c). It should be noted that even under 0.25 sun illumination (conforming to the real outside condition), the evaporation rate was about 0.30 kg m^{-2} h^{-1} and the efficiency remained at 81.7%, higher than that of most literature studies reported under low solar flux (<1 sun).[46–48] These results carry more significance for real industrial applications owing to no costly and complicated optical concentration equipment. The evaporation rate increased with the increase of solar intensity, and the efficiency was up to 92.1% with an evaporation rate of 7.02 kg m^{-2} h^{-1} under 5 sun.

3.5 Reusability of carbon bread

Stability is an important and practical factor for the outdoor use of solar desalination devices.[49] The dry state carbon bread could be stored for a long time (6 months) and was ready for use without spoiling (Fig. S10a†). It is worth noting that the CB-6 still exhibited stable conversion efficiency after 200 hours (Fig. 5d), suggesting the excellent stability of the device. To evaluate the reusability during desalination, saline water with 3.5 wt% NaCl (mimicking the seawater) was prepared for the solar water evaporation experiment repeatedly using the same sample (details are given in the ESI†). As

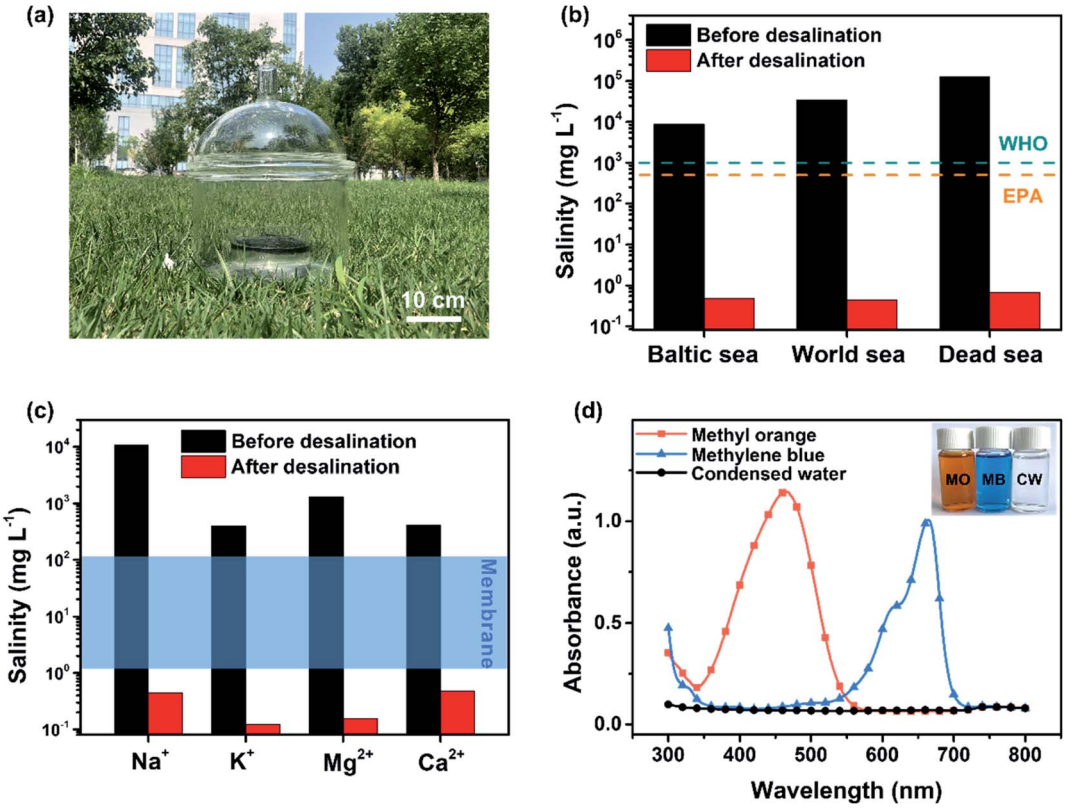

Fig. 6 (a) Outdoor solar water desalination and purification device under natural sunlight. (b) The salinity of three seawater samples and (c) measured concentrations of ions before and after desalination. (d) The UV-Vis spectra of methyl orange (MO) and methylene blue (MB) solutions before and after solar sewage treatment.

shown in Fig. 5e, the evaporation rates with saline water were stable under 1 sun illumination for 15 cycles, demonstrating the fine stability and reusability of CB-6. After 15 cycles, the material was washed and the structure was characterized, showing that the structure barely changed and no NaCl crystal was deposited on the material after desalination and washing (Fig. S10b†), ready for the next use. Meanwhile, a long-time test over 9 hours was also carried out (Fig. S11†) and the rate remained nearly unchanged.

3.6 Demo application

A solar evaporator using carbon bread (diameter: 15 cm and thickness: 1 cm) for outdoor use is presented in Fig. 6a and S12.†

Three representative simulated seawater samples (NaCl solution) of different salinities were prepared, including the Baltic Sea (0.8 wt%), the World Ocean (3.5 wt%) and the Dead Sea (10 wt%). The Na^+ concentrations of the simulated seawater and desalinated water were tested by ICP-MS, and the results are shown in Fig. 6b. All the desalinated water samples showed extremely low salinity, at least a 4 orders of magnitude decrease, meeting the drinkable water standards defined by the World Health Organization (WHO) and the US Environmental Protection Agency (EPA).[13,50] Further, the simulated seawater samples with four primary ions (Na^+, K^+, Mg^{2+} and Ca^{2+}) were then used for testing. As shown in Fig. 6c, all the concentrations significantly decreased below 0.5 mg L^{-1} after desalination, much lower than that of reverse osmosis based seawater desalination. Meanwhile, the same method was applied to obtain freshwater from the sewage water with methyl orange (MO) or methylene blue (MB). As presented in Fig. 6d, the quality of the generated freshwater after treatment was verified using optical absorption spectroscopy measurements, which showed that the water contained no contaminant MO or MB as evidenced by the near-zero optical absorbance.

4. Conclusion

In this work, we fabricated porous carbon bread *via* a simple, cost-effective and scalable manufacturing process that can be carried out in most household kitchens and can realize fully automatic production. The as-prepared carbon bread exhibited excellent properties as an optimal solar absorber, including >98% solar absorption in 200–2500 nm, 3D interconnected hierarchical pores, hydrophilic structures and low thermal conductivity. Therefore, when directly used as an evaporator for solar steam generation, the optimal carbon bread exhibited a high solar conversion efficiency of 85.9% under 1 sun and >81% even under ambient sunlight (<1 sun). Thus, by employing this material, we can concurrently achieve highly efficient solar-driven water desalination and purification. This work not only reveals the hidden potential of carbon bread for efficient solar steam generation but also

provides a new route to design and fabricate scalable, low-cost and high-performance solar-thermal conversion devices for practical applications.

Conflicts of interest

There are no conflicts of interest to declare.

Acknowledgements

The authors gratefully acknowledge the financial support from the National Natural Science Foundation of China (No. 51902360) and the Special Fund for Basic Scientific Research Business of Central Public Research Institutes (K-JBYWF-2019-CR01, Y-JBYWF-2019-15).

References

1 J. Eliasson, *Nature*, 2015, **517**, 6.
2 M. Elimelech and W. A. Phillip, *Science*, 2011, **333**, 712–717.
3 M. A. Shannon, P. W. Bohn, M. Elimelech, J. G. Georgiadis, B. J. Marinas and A. M. Mayes, *Nature*, 2008, **452**, 301–310.
4 W. Shang and T. Deng, *Nat. Energy*, 2016, **1**, 16133.
5 P. Zhang, Q. Liao, H. Yao, Y. Huang, H. Cheng and L. Qu, *Energy Storage Maters*, 2019, **18**, 429–446.
6 P. Tao, G. Ni, C. Song, W. Shang, J. Wu, J. Zhu, G. Chen and T. Deng, *Nat. Energy*, 2018, **3**, 1031–1041.
7 L. Zhou, X. Li, G. W. Ni, S. Zhu and J. Zhu, *Natl. Sci. Rev.*, 2019, **6**, 562–578.
8 X. Hu and J. Zhu, *Adv. Funct. Mater.*, 2020, **20**, 1907234.
9 H. Liu, Z. Huang, K. Liu, X. Hu and J. Zhou, *Adv. Energy Mater.*, 2019, **9**, 1900310.
10 T. Wei, X. Li, J. Li, L. Zhou, S. Zhu and J. Zhu, *Chin. Sci. Bull.*, 2018, **63**, 1405–1416.
11 V. Kashyap and H. Ghasemi, *J. Mater. Chem. A*, 2020, **8**, 7035–7065.
12 F. Zhao, X. Zhou, Y. Shi, X. Qian, M. Alexander, X. Zhao, S. Mendez, R. Yang, L. Qu and G. Yu, *Nat. Nanotechnol.*, 2018, **13**, 489–495.
13 L. Zhou, Y. Tan, J. Wang, W. Xu, Y. Yuan, W. Cai, S. Zhu and J. Zhu, *Nat. Photonics*, 2016, **10**, 393–398.
14 H. Ghasemi, G. Ni, A. M. Marconnet, J. Loomis, S. Yerci, N. Miljkovic and G. Chen, *Nat. Commun.*, 2014, **5**, 4449.
15 K. Bae, *Nat. Commun.*, 2015, **6**, 10103.
16 L. Zhou, S. Zhuang, C. He, Y. Tan, Z. Wang and J. Zhu, *Nano Energy*, 2017, **32**, 195–200.
17 X. Fan, Y. Ding, Y. Liu, J. Liang and Y. Chen, *ACS Nano*, 2019, **13**, 8124–8134.
18 L. Zhou, Y. Tan, D. Ji, B. Zhu, P. Zhang, J. Xu, Q. Gan, Z. Yu and J. Zhu, *Sci. Adv.*, 2016, **2**, e1501227.
19 Y. Yang, R. Zhao, T. Zhang, K. Zhao, P. Xiao, Y. Ma, P. M. Ajayan, G. Shi and Y. Chen, *ACS Nano*, 2018, **12**, 829–835.
20 X. Li, W. Xu, M. Tang, L. Zhou, B. Zhu, S. Zhu and J. Zhu, *Proc. Natl. Acad. Sci. U. S. A.*, 2016, **113**, 13953–13958.
21 H. Ren, M. Tang, B. Guan, K. Wang, J. Yang, F. Wang, M. Wang, J. Shan, Z. Chen, D. Wei, H. Peng and Z. Liu, *Adv. Mater.*, 2017, **29**, 1702590.
22 J. Wang, Y. Li, L. Deng, N. Wei, Y. Weng, S. Dong, D. Qi, J. Qiu, X. Chen and T. Wu, *Adv. Mater.*, 2016, **29**, 1603730.
23 Y. Zeng, J. Yao, B. A. Horri, K. Wang, Y. Wu, D. Li and H. Wang, *Energy Environ. Sci.*, 2011, **4**, 4074–4078.
24 M. Zhu, Y. Li, G. Chen, F. Jiang, Z. Yang, X. Luo, Y. Wang, S. D. Lacey, J. Dai, C. Wang, C. Jia, J. Wan, Y. Yao, A. Gong, B. Yang, Z. Yu, S. Das and L. Hu, *Adv. Mater.*, 2017, **29**, 1704107.
25 N. Xu, X. Hu, W. Xu, X. Li, L. Zhou, S. Zhu and J. Zhu, *Adv. Mater.*, 2017, **29**, 1606762.
26 F. Chen, A. S. Gong, M. Zhu, G. Chen, S. D. Lacey, F. Jiang, Y. Li, Y. Wang, J. Dai, Y. Yao, J. Song, B. Liu, K. Fu, S. Das and L. Hu, *ACS Nano*, 2017, **11**, 4275–4282.
27 J. Guan and M. A. Hanna, *Bioresour. Technol.*, 2006, **97**, 1716–1726.
28 Q. Zhang, H. Yang, X. Xiao, H. Wang, L. Yan, Z. Shi, Y. Chen, W. Xu and X. Wang, *J. Mater. Chem. A*, 2019, **7**, 14620–14628.
29 S. Liu, C. L. Huang, Q. Q. Huang, F. C. Wang and C. W. Guo, *J. Mater. Chem. A*, 2019, **7**, 17954–17965.
30 N. Li, L. Qiao, J. He, S. Wang, L. Yu, P. Murto, X. Li and X. Xu, *Adv. Funct. Mater.*, 2020, 2008681.
31 L. Yang, G. Chen, N. Zhang, Y. Xu and X. Xu, *ACS Sustainable Chem. Eng.*, 2019, **7**, 19311–19320.
32 L. Yang, N. Li, C. Guo, J. He, S. Wang, L. Qiao, F. Li, L. Yu, M. Wang and X. Xu, *Chem. Eng. J.*, 2020, DOI: 10.1016/j.cej.2020.128051.
33 X. Zhou, F. Zhao, Y. Guo, B. Rosenberger and G. Yu, *Sci. Adv.*, 2019, **5**, eaaw5484.
34 Y. Zhang, X. Y. Yin, B. Yu, X. L. Wang, Q. Q. Guo and J. Yang, *ACS Appl. Mater. Interfaces*, 2019, **11**, 32559–32568.
35 Y. Ito, Y. Tanabe, J. Han, T. Fujita, K. Tanigaki and M. Chen, *Adv. Mater.*, 2015, **27**, 4302–4307.
36 P. Xiao, J. C. Gu, C. Zhang, F. Ni, Y. Liang, J. He, L. Zhang, J. Y. Ouyang, S. W. Kuo and T. Chen, *Nano Energy*, 2019, **65**, 104002.
37 T. Li, H. Liu, X. Zhao, G. Chen, J. Dai, G. Pastel, C. Jia, C. Chen, E. Hitz, D. Siddhartha, R. Yang and L. Hu, *Adv. Funct. Mater.*, 2018, **28**, 1707134.
38 Z. Liu, H. Song, D. Ji, C. Li, A. Cheney, Y. Liu, N. Zhang, X. Zeng, B. Chen, J. Gao, Y. Li, X. Liu, D. Aga, S. Jiang, Z. Yu and Q. Gan, *Global Challenges*, 2017, **1**, 1600003.
39 M. Ye, K. Zhu, J. Gao, R. Chen and T. Zhang, *Water Sci. Technol.: Water Supply*, 2019, **19**, 1938–1944.
40 Y. Liu, J. Chen, D. Guo, M. Cao and L. Jiang, *ACS Appl. Mater. Interfaces*, 2015, **7**, 13645–13652.
41 T. Chen, S. Wang, Z. Wu, X. Wang, J. Peng, B. Wu, J. Cui, X. Fang, Y. Xie and N. Zheng, *J. Mater. Chem. A*, 2018, **6**, 14571–14576.
42 B. Lagrain, K. Brijs and J. A. Delcour, *J. Agric. Food Chem.*, 2008, **56**, 10660–10666.
43 J. B. Engel, A. Ambrosi and I. C. Tessaro, *Carbohydr. Polym.*, 2019, **225**, 115234.
44 Y. Geng, K. Zhang, K. Yang, P. Ying, L. Hu, J. Ding, J. Xue, W. Sun, K. Sun and M. Li, *Carbon*, 2019, **155**, 25–33.

45 P. Qiu, F. Liu, C. Xu, H. Chen, F. Jiang, Y. Li and Z. Guo, *J. Mater. Chem. A*, 2019, **7**, 13036–13042.
46 G. Ni, S. H. Zandavi, S. M. Javid, S. V. Boriskina, T. A. Cooper and G. Chen, *Energy Environ. Sci.*, 2018, **11**, 1510–1519.
47 Y. Zhang, S. K. Ravi, L. Yang, J. V. Vaghasiya, L. Suresh, I. Tan and S. Tan, *ACS Appl. Mater. Interfaces*, 2019, **11**, 38674–38682.
48 X. Wu, Q. Jiang, D. Ghim, S. Singamaneni and Y. Jun, *J. Mater. Chem. A*, 2018, **6**, 18799–18807.
49 X. Bai, Y. Li, F. Zhang, Y. Xu, S. Wang and G. Fu, *Environ. Sci.: Water Res. Technol.*, 2019, **5**, 2041–2047.
50 Q. Gan, T. Zhang, R. Chen, X. Wang and M. Ye, *ACS Sustainable Chem. Eng.*, 2019, **7**, 3925–3932.